Dynamic Battery Package System Simulation and Layout Optimization

BY

Chongye Wang
B.Eng., Tianjin University of Commerce, Tianjin, P.R.China, 2010

THESIS

Submitted as partial fulfillment of the requirements
for the degree of Master of Science in Industrial Engineering
in the Graduate College of the
University of Illinois at Chicago, 2013

Chicago, Illinois

Defense Committee:

Dr. Lin Li, Chair and Advisor
Dr. Jeremiah T. Abiade
Dr. David He

ACKNOWLEDGMENTS

I would like to thank my advisor, Dr. Lin Li, Assistant Professor in the Department of Mechanical and Industrial Engineering, University of Illinois at Chicago, for his valuable guidance and support throughout the thesis project. No words can express my gratitude for his open of the door of Sustainable Manufacturing Systems Research Laboratory to me. I also wish to thank him for mentoring me not only academically but all other aspects which will be beneficial for all my lifetime.

I would also like to thank Dr. Jeremiah T. Abiade and Dr. David He for serving as part of my graduate committee. Their valuable guidance during the project and other generous help are greatly appreciated.

I wish to thank all the other lab mates, Dr. Yong Wang, Mr. Zeyi Sun, Mr. Zhichao Zhou, Ms. Mayela Fernandez, Mr. Andres Bego, Mr. Haoxiang Yang and Mr. Josh Reese. The study and life in the Sustainable Manufacturing Systems Research Laboratory could not be delighted without the collaboration with them.

Finally, I wish to thank my parents, Mr. Xuanya Wang and Mrs. Liya Zhang. I would never have the opportunity to study in the United States without the unwavering support and assistance of them.

TABLE OF CONTENTS

CHAPTER PAGES

LIST OF FIGURES

FIGURE PAGE

LIST OF TABLES

TABLE PAGE

LIST OF ABBREVIATIONS

BPS	Battery Package System
BFS	Brute Force Search
CE	Combustion Engine
EV	Electric Vehicle
EIA	Energy Information Administration
EPA	Environment Protection Agency
GHG	Green House Gas
HEV	Hybrid Electric Vehicle
SOC	State-of-Charge
SOH	State-of-Health
TBPD	Thousands Barrels Per Day

SUMMARY

Due to the increasing energy demand and Greenhouse Gas (GHG) emission in recent decades, the significance of environmental protection has been widely realized by both academia and industry. More and more companies are trying to shift their traditional profit-focused operation mode to a more sustainable one that jointly considers the economic, environmental, and ecological aspects. The "green" products have been increasingly popular to the customers due to the adoption of different environment-friendly methods.

Electric Vehicle (EV) is thought to be a good example of "green" product which is expected to replace the traditional Combustion Engine (CE) vehicle by using Battery Package System (BPS) to power the vehicle. Unlike the battery systems for portable electronic devices using single or a few cells, the number of cells for the large load such as EV is very huge. Therefore, the manufacturing processes and designed layouts are much more complex, which play a critical role in the battery performance in terms of both functionality and cost.

The **objective** of this thesis is to 1) develop a simulation model for the functionality performance evaluation by obtaining different profiles of working dynamics for the BPS considering the manufacturing processes; and 2) establish a cost-effective layout design model to minimize the overall cost under the performance constraint with respect to satisfying the demand.

1. INTRODUCTION

The crude oil consumption of U.S. mainland increased by 17.4% from 5091 TBPD in 2011 to 5979 TBPD in 2012, about 23.3% increment compared with 2000 (EIA 2013). About 6,702 million metric tons carbon dioxide, the main constituent of Greenhouse Gas (GHG), was emitted in 2011 as shown in Figure 1 (EPA 2013).

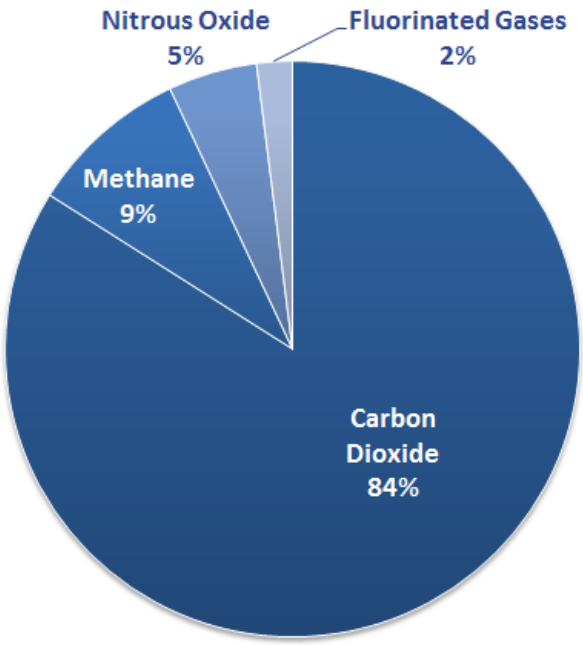

Figure 1 U.S. Greenhouse Gas Emission in 2011, totally 6,702 million metric tons CO2 equivalent. Source: (EPA 2013)

Among the huge volume of total GHG emissions, the transportation sector dominated by traditional combustion engine (CE) vehicles is the second largest GHG emitter in terms of end-use sector, which is responsible for about 28% of the total emissions (see Figure 2).

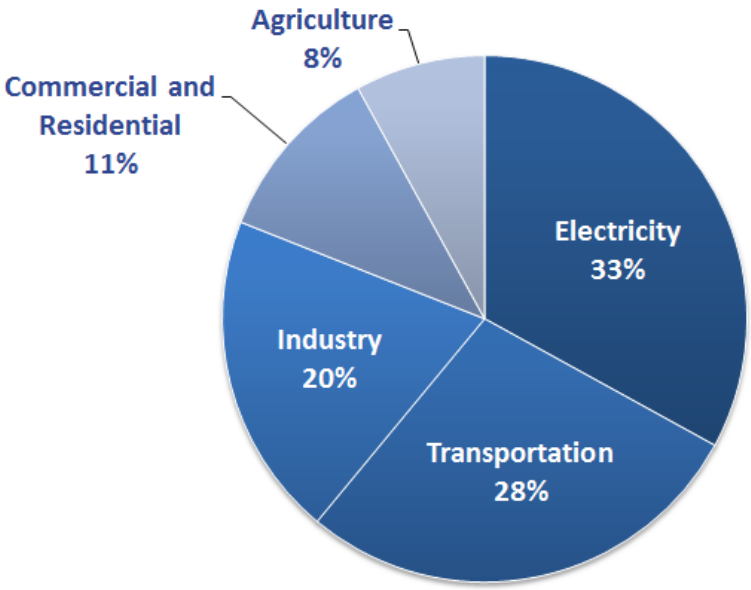

Figure 2 Total U.S. Greenhouse Emissions by Economic Sector in 2011. Source: (EPA 2013)

The development of the technology focusing on new power source to replace the traditional fossil fuel for vehicles has become a very popular and interesting topic to both academia and industry. The Battery Pack System (BPS) is considered a promising technology to replace the CE system due to the following two major advantages: 1) electricity can be generated from the renewable energy sources like solar, wind, water, tide, and geotherm, which can decrease the GHG emission compared with fossil fuel; and 2) the working noise of BPS is much lower than CE, which can bring a more comfortable driving environment for the drivers. A BPS generally consists of multiple battery cells based on the demand of the equipment or application. Different types of batter cells with different chemical components, i.e., Nickel Cadmium (NiCd), Nickel-Metal Hydride (NiMH), Lead-Acid, and Lithium-ion (Li-ion) can be chosen.

In last couple of decades, Hybrid Electric Vehicles (HEV) had firstly attracted wide attention. It was once the main objective of the most research in EV area. The battery systems of HEV are focused on the NiMH, Lead-Acid and NiCd battery. Although HEV has a battery system which can power the vehicle, the major power is still supplied by combustion engine. The battery system is just used as an alternate power supplier when the vehicle is on low load demand or under specific emergency like no available gasoline. It can only support for short durations and miles.

To power the vehicle by electricity entirely, the material of the battery cells need a high energy density. Recently, due to the technology development on material, chemistry, and electronics, the Lithium-ion (Li-ion) battery has been gradually emerged in the market with its higher energy density. It has drawn public's attention due to its better energy performance and light weight. According to the investigation report from General Motor (GM) (SAE Magazine 2010), compared with the pack of NiMH, Li-ion pack can have up to three times energy density (110-130 W·h/kg) in a much smaller package. Li-ion cells are also more configurable and prone to less self-discharge when they are not in use. In addition, they are potentially less expensive. Figure 3 shows a Li-ion cell used for EV BPS.

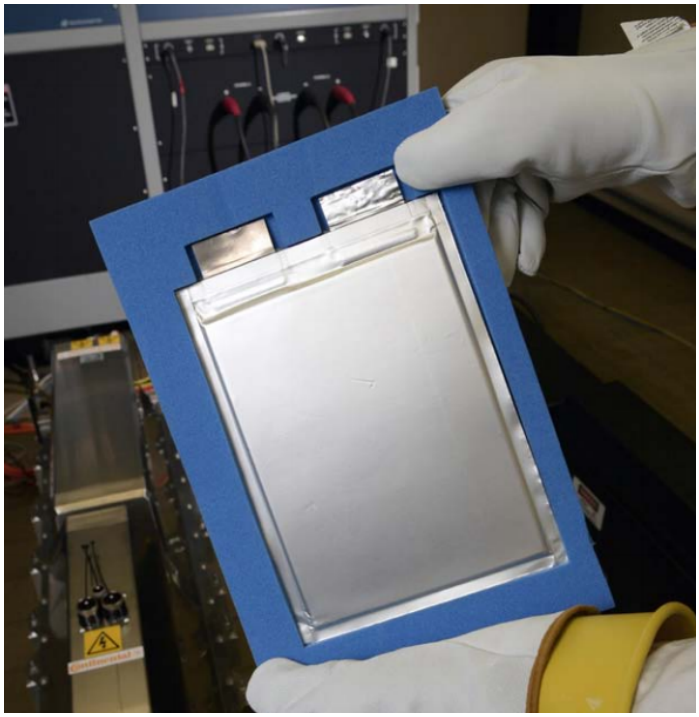

Figure 3 Single Li-ion Battery Cell. Source: (SAE Magazine 2010)

Generally, the BPS may contain lots of battery cells, for example, the T-shape BPS in Volt produced by GM includes totally 288 Li-ion cells (SAE Magazine 2010). Each cell has to be properly designed and connected on right position to save the system space as well as the package weight. The appropriate number of the cells included in the whole pack and the influence of the different manufacturing processes on the battery performance need be identified to satisfy the desired level of the probability that the BPS can satisfy the demand (SAE Magazine 2010). However, a brief review on Li-ion battery research for EV has revealed that most research efforts in this area are on cell-level electrochemistry and new materials development (Girishkumar, G. et al. 2010; Aifantis, K. E. et al. 2007), dynamics and simulation (Tremblay, O. 2009; Jossen, A. 2006; Johnson, B. A. 1998), charging or discharging equalization (Kaiser, R. 2007; Miller, G. 2006; Plett, G. 2004), and environmental impact and sustainability (Bradley, T.

H. and Frank, A. A. 2009; Karner, D. and Francfort, J. 2007), but few on the pack-level battery performance evaluation considering manufacturing process and the layout optimization considering cost effectiveness. In practice, every process in the battery pack manufacturing system will affect the performance of the final BPS. Due to the variations in the manufacturing process, it is unlikely that every battery pack will behave the same. Although there are a few studies which mention cell pack framework and the layout design (Jossen, A. 2006; Ju, F. et al. 2011), none of them show the details on how to connect the cell, in series or parallel, and what the results of the performance in terms of functionality such as charging-discharging and the overall cost are.

In this thesis, we will first investigate the influences of the manufacturing process on the final battery pack performance by developing a simulation model on the whole pack level to obtain different profiles describing working dynamics. After that, optimal layout design of the BPS will be focused considering the overall cost performance under the constraint of the desired level of the probability to satisfy the demand. The rest part of the thesis is organized as follows. In Chapter 2, the basic mechanism of battery as well as terminology used in battery realm will be introduced as a foundation for the later chapters. Chapter 3 will introduce the simulation model that can evaluate the pack level battery performance considering the manufacturing processes. It includes the introduction about different cell connections, i.e. serial and parallel cell connections, and how this connection is conducted in the simulation model. Chapter 4 will introduce an optimal layout design model for BPS for the purpose of cost effectiveness. Finally, Chapter 5 will conclude the thesis and propose the future work.

2. BATTERY BACKGROUND INFORMATION

In this chapter, we will first give a brief review on the history of the battery. After that, the basic mechanisms of battery system will be outlined and the terminologies will be introduced. Finally, several typical battery types will be briefly introduced. This chapter is served as a foundation for the later chapters in this thesis.

2.1 Battery history

The term "battery" was first coined by Benjamin Franklin in 1748 (Wikipedia 2013). In 1800, Volta invented the first "wet cell battery" that produced a reliable, steady current of electricity (Wikipedia 2013). In 1859, the first-ever rechargeable Lead-acid battery was discovered, and then the dry cell was presented in 1899 by several battery developers (Wikipedia 2013).

In late 19th century and early 20th century, the battery using Nickel-cadmium (NiCd) and Nickel-iron, which are the so-called "dry cell", obtained the public attention. It became a substitute of Zinc-carbon battery after 1950s due to its long life time as well as the high energy density. Since 1989, the nickel-metal hybrid battery (NiMH) has emerged and gradually replaced NiCd battery due to its longer lifespan and less toxic,

In recent decades, the Lithium-ion (Li-ion) battery has been proven the ideal material for batteries not only due to its lower weight but also the greatest electrochemical potential compared to other materials. Since 1997, the Lithium-ion polymer battery has dominated almost the entire battery market. These batteries hold their electrolyte in a solid polymer composite

instead of a liquid solvent and the electrodes and separators are laminated to each other, the latter difference allows the battery to be encased in a flexible wrapping instead of a rigid metal casing. This gives Li-ion battery the ability that can be specifically shaped to fit a particular device.

2.2 Battery Configuration

2.2.1 Electrode

An electrode is usually an electrical conductor. In battery it refers to the anode and cathode. When reacting with electrolyte, the anode will lose its electrons and transfer them to cathode by the external circuit and form the current which can support the load. The materials for electrode are metal and oxide.

2.2.2 Electrolyte

Electrolyte is a compound that can conduct electricity when dissolved in suitable solvents such as water. When electrodes are placed in electrolyte and a voltage is applied, the electrolyte will be able to conduct electricity. Single electron normally cannot pass through the electrolyte, instead, a chemical reaction occurs at the cathode consuming electrons from anode; another reaction occurs at the anode producing electrons that are transferred to cathode eventually. Consequently, a negative charge is developed in the electrolyte around cathode and a positive charge is developed around anode. The ions in the electrolyte neutralize these charges and enable the electrons to keep flowing and the reaction to continue.

2.2.3 Separator

A separator is used to isolate electrodes so that short-circuit can be avoided. An effective separator must possess a number of mechanical properties such like permeability, porosity, strength, electrical resistance, ionic conductivity and chemical compatibility with electrolyte.

2.3 Battery Terminology

Voltage (V)

Voltage in battery refers to the difference between the battery electrodes (i.e. the difference between anode and cathode. In general, voltage is electric potential energy per unit of charge, measured in joules per coulomb (Volts).

Current (I)

Current is a flow of electric charge when there is voltage present across a conductor/load. In battery, the current flows from positive plate to negative plate during discharging and from negative to positive while charging, measured in ampere (A).

Capacity (C)

Battery capacity is the amount of electric charge that can be stored in one battery. When the chemical materials are the same, the more electrode and electrolyte may lead to the greater capacity. The available capacity of a battery depends on the discharging rate, if the battery

discharges at a relatively high rate, the available capacity will be lower than expected. For example, a 10Ah battery rated at 0.2C (i.e. deliver a 2A current) can discharge 5 hours, however, if it discharges at 1C (i.e. deliver a 10A current), it will have a lower discharging period (1 hour). Also, the discharge condition such like the magnitude of current, the allowable terminal voltage of the battery, temperature and other factors can affect the battery capacity. Usually, the unit of capacity is Ah or mAh.

State of Charge (SOC)

State of Charge is the gauge for the battery pack in an EV or HEV. The units of SOC are represented in percentage points (i.e. 0%=empty, 100%=full).

State of Health (SOH)

State of Health is the performance level of the battery compared to its ideal condition. The units of SOH are represented in percentage points (i.e. 100%=the battery's conditions match the battery's specification).

Primary Battery

Primary Battery refers to the non-rechargeable battery. It can only be used once and the chemical reaction inside the battery is not reversible. Primary battery also be called disposable battery.

Secondary Battery

Secondary Battery refers to the rechargeable battery which can be used again after a fully discharging, the chemical reaction inside a secondary battery is electrically reversible. Secondary battery is expected to have lower total cost of use and environment impact than primary battery.

2.4 Battery Types and Mechanism

2.4.1 Lead-Acid Battery

Lead-Acid battery is the first rechargeable battery which was introduced in 1859 by French physicist Gaston Plante. Despite of its pretty low energy-weight ratio as well as energy-volume ratio, Lead-Acid battery can supply a high surge current. This implies it can maintain a relatively large power-weight ratio which makes it capable for using in combustion vehicles to provide the high current required by ignition system. Lead-Acid battery use lead (Pb) as both of its plates, anode and cathode, to react with sulfate to lose electrons for discharging, and gain electrons from power supply for charging to complete the discharge-charge circle. Figure 4 and 5 demonstrate the basic working mechanism of Lead-Acid battery.

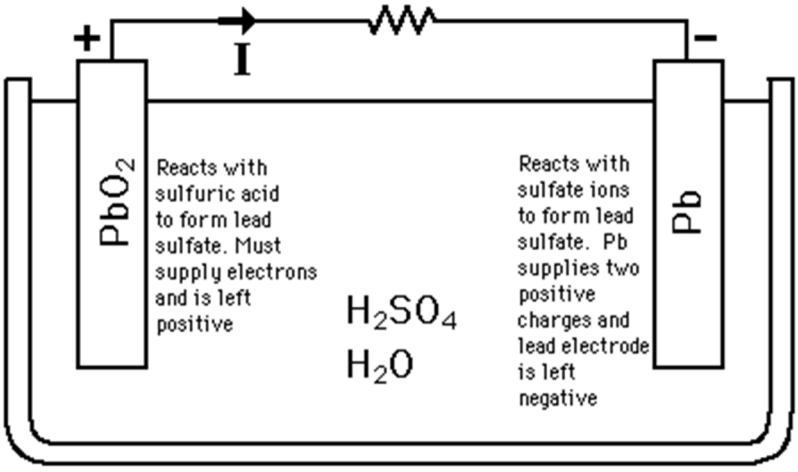

Figure 4 Lead-Acid Battery Mechanism: Discharging. Source: (Google Images 2013)

For the discharging process, the negative plate (Anode) will react with H_2SO_4 and generate electrons and $PbSO_4$, the electrons will be transferred to positive plate through the external circuit connecting with a load, the current is issued from positive plate to negative.

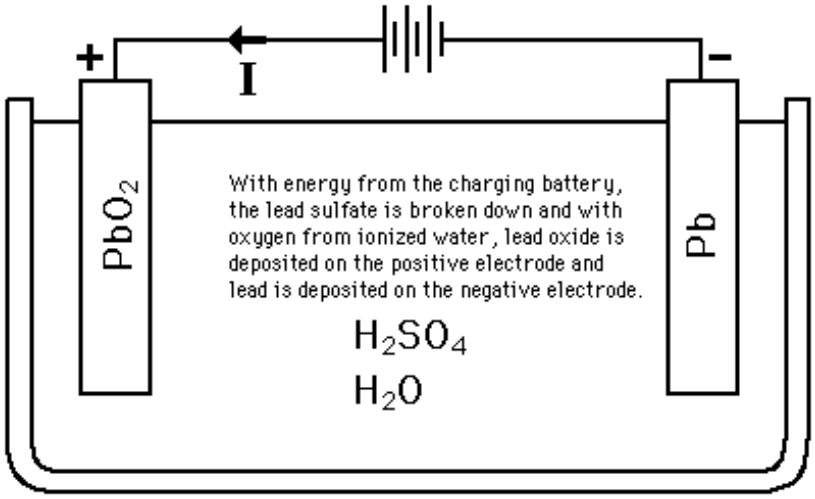

Figure 5 Lead-Acid Battery Working Mechanism: Charging. Source: (Google Images 2013)

For the charging process, the $PbSO_4$ on positive plate (Cathode) will react with H_2O to release electrons, these electrons will be gathered by negative plate and become Pb again.

A separator, which is not showing in the figures, is placed between anode and cathode to avoid short-circuit through physical contact.

2.4.2 Nickel-Cadmium Battery

NiCd battery is the first battery use alkaline electrolyte which appears in 1899. Same as Lead-Acid, NiCd is a so called "wet cell" battery because they have liquid electrolyte inside the battery. The difference is NiCd battery use nickel as its positive plate and cadmium as the negative plate. These new reaction materials give NiCd battery higher energy density and also the more robust physical and chemical performance than Lead-Acid battery.

The separator isolates negative and positive plates are rolled in a spiral shape inside the case, this is known as the Jelly-Roll design and relatively enlarge the contact surface between electrode and electrolyte so that the NiCd cell can deliver much high maximum current. Figure 6 shows the configuration of a typical NiCd battery.

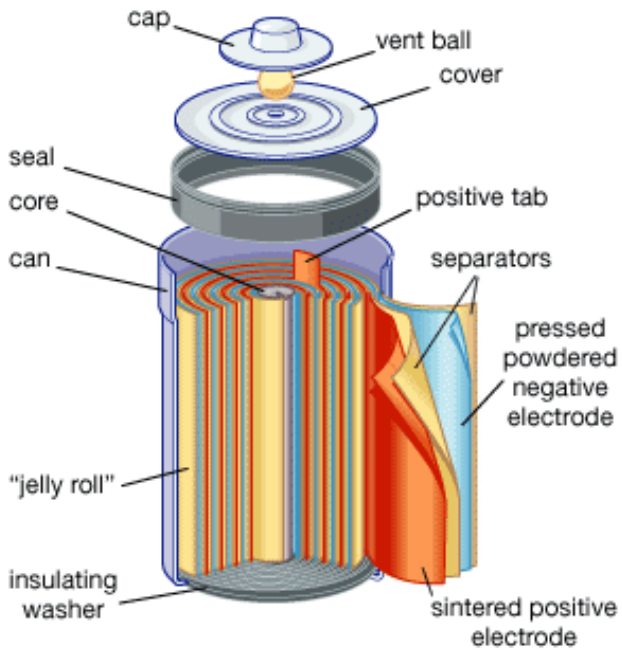

Figure 6 NiCd Battery Configuration. Source: (Google Images 2013)

The biggest also most well-known problem of NiCd battery is the "Memory Effect". When it suffers from discharging and charging to the same State of Charge (*SOC*) hundreds of times, NiCd battery apparent symptom is that the battery "remember" the point in its discharge-charge circle where recharging begins and during subsequent use suffers a sudden drop in voltage at that point, as if the battery has been depleted, though the actual capacity of the battery is not reduced substantially. Some electronics or systems powered by NiCd battery are able to withstand this reduced voltage long enough for the voltage to recover, however, if the device is unable to operate through this period under this decreased voltage, the battery will be judged as "dead" earlier than normal.

Despite the "Memory Effect" problem and the toxic property of cadmium, NiCd battery got an overwhelming majority of the battery market during the mid-1990s.

2.4.3 Nickel-metal Hybrid Battery

Basically, NiMH battery is very similar with NiCd battery, the positive plate is the nickel oxy-hydroxide just like NiCd, but the negative plate is hydrogen-absorbing alloy instead of cadmium be the essential reaction chemistry. This gives NiMH battery two advantages, one is higher energy density and the other is less environment hazard. Usually, a NiMH can have two to three times capacity of an equivalent size NiCd battery.

NiMH battery has been successfully applied into EV such like General Motor EV1 and Dodge Caravan EPIC minivan.

2.4.4 Lithium-ion Battery

The first thing need to make clear is Li-ion battery is different from Lithium battery, most people mix these two kinds of battery together, but the truth is Lithium battery is unstable and dangerous to be used in daily life. Generally, a Lithium-ion battery is rechargeable by using an intercalated lithium compound as the electrode compared with metallic lithium used in non-rechargeable lithium battery.

Li-ion battery has been widely used in various applications not only in electronics, but also in automotive industry, military and aerospace areas. Due to its high energy density, memory less attribute and low self-discharge rate, Li-ion battery is growing in popularity, and becomes a

common replacement of Lead-Acid battery. It uses graphite as the anode and lithium oxide compound as the cathode. Because pure lithium is highly reactive and it can react with water to form lithium hydroxide and hydrogen gas, so the electrolyte usually be used for Li-ion battery is a non-aqueous lithium salt in an organic solvent, and a sealed container rigidly excludes moisture is required. Figure 7 shows the basic mechanism of Li-ion battery.

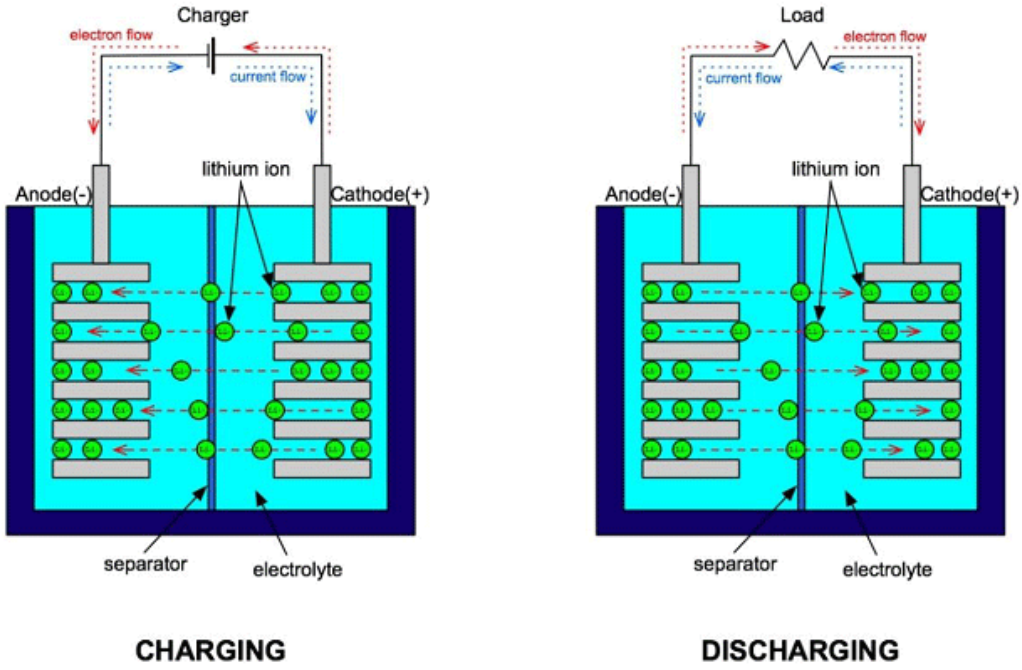

Figure 7 Lithium-ion Battery Working Mechanism. Source: (Google Images 2013)

Li-ion battery has several other advantages comparing with other rechargeable batteries like Lead-Acid and NiCd. It can operate over a wide temperature range with higher energy density than NiCd battery, and also it has longer life cycles due to non-memory-less effect, meanwhile, Li-ion battery is using a non-toxic material as electrodes so it is said no hazard to environment.

However, of course, Li-ion battery has some disadvantages. The battery uses a flammable material as its electrolyte and also be kept in pressure, this makes the manufacturing standard of these batteries high and consists of many safety features. The flammable material inside can lead to a battery fire or explosion due to improperly use.

3. MODELING ALGORITHM OF BATTERY PACKAGE SYSTEM

3.1 Motivation

A battery system consisting of two or more battery cells can be treated as a Battery Package System (BPS). The number of cells in the BPS depends on the load. Generally, for portable devices or electronic equipment, the BPS only contains very few cells. For example, a BPS for a laptop may only contain 6 cells. However, for the large load application such as electric vehicles, the cell number will raise to several hundreds. For example, Volt, the EV of GM is powered by a BPS consisting of 288 Li-ion battery cells (SAE Magazine 2010). Figure 8 is a real Volt battery package system.

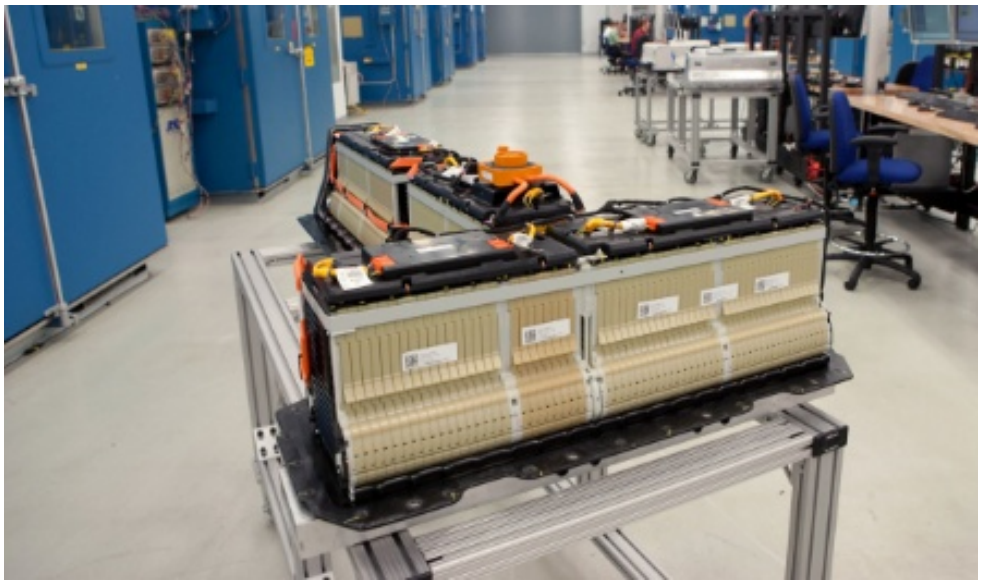

Figure 8 Volt Battery Package System. Source: (Google Images 2013)

In practice, EV batteries may not be ideally manufactured. This chapter proposes a novel simulation-based modeling method for analyzing the effects of manufacturing processes on the dynamics of EV Li-ion battery packs. The method will help engineers gain a deeper understanding of the roles of manufacturing processes in improving EV Li-ion battery performance.

3.2 Dynamics Modeling of Single Cells

For a single battery cell, the most important dynamical characteristics are Voltage (*V*), Current (*I*) and State-of-Charge (*SOC*). There are many publications on Li-ion battery cell dynamics modeling (Martínez-Rosas, E et al. 2011; Shepherd, C. M. 1965; Chen, M 2006; Knauff, M 2007; Tremblay, O and Dessaint, L. A 2007). Generally, they all try to model the relationships between *V*, *I* and *SOC*. Figure 9 shows a typical discharging/charging curve of V and SOC. The beginning of the discharging behavior (a) presents a sharp drop or exponential area, and then it comes to a nominal area (b), where the voltage does not change a lot to offer a stable voltage for load. At the end of the nominal area (c), because the charge in the battery has exhausted, the voltage begins to drop sharply again until it reaches the cut-off level.

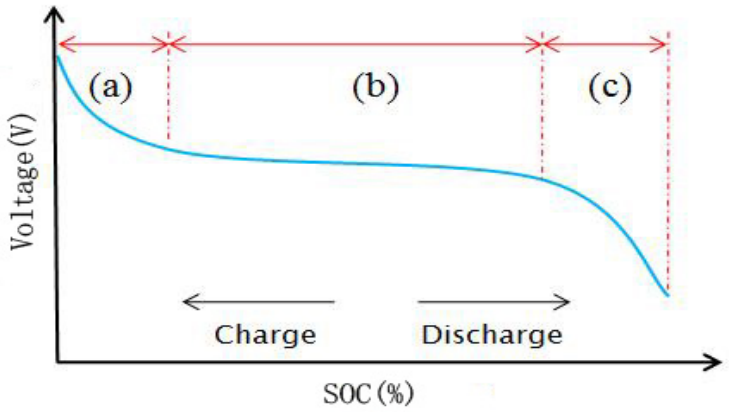

Figure 9 Typical Discharge-charge curve

The single-cell model presented in this paper is based on (Tremblay, O and Dessaint, L. A 2007 & 2009), which is a modified type of Shepherd's model using polarization voltage instead of polarization resistance (Shepherd, C. M. 1965). This model is adopted in this paper because it is specifically validated for EV applications. The dynamics of the cell voltage when discharging and charging can be expressed by the following equations in (Tremblay, O and Dessaint, L. A 2009).

Discharging:

$$V = E_0 + a \cdot e^{-b \cdot D} - I \cdot R - I \cdot k \frac{Q}{Q - D} \tag{3.1}$$

Charging:

$$V = E_0 + a \cdot e^{-b \cdot D} - I \cdot R - I \cdot k \frac{Q}{D + 0.1Q} \tag{3.2}$$

where

E_0= the base voltage

I= current

R= internal resistance

Q = battery capacity

D = used capacity, denoted by $it = \int idt$

$a,\ b$ = empirical constants

k = polarization constant

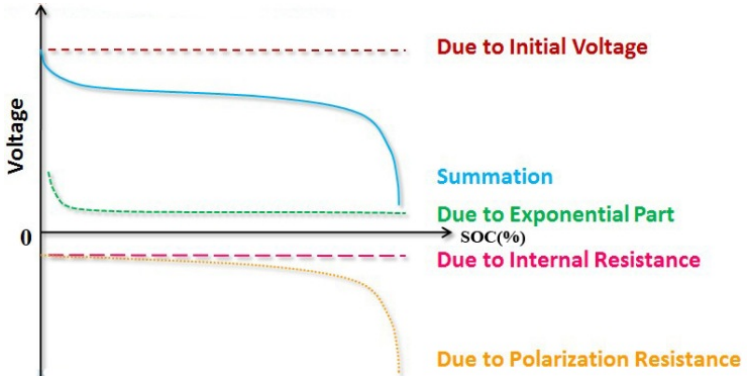

Figure 10 Decomposition of the Typical Discharge Curve

Amid these equations, according to Tremblay and Dessaint (Tremblay, O and Dessaint, L. A 2007 & 2009), $a \cdot e^{-b \cdot D}$ represents the exponential part in Figure 9; $I \cdot R$ represents the voltage due to internal resistance, while $I \cdot k \frac{Q}{Q - D}$ illustrates the voltage caused by polarization resistance. According to Tremblay (Tremblay, O and Dessaint, L. A 2007), when D=0, which means the battery is fully charged, the polarization resistance is infinite. Therefore, during the charging state, we rewrite the last part of the discharging equation by using $I \cdot k \frac{Q}{D + 0.1Q}$, which is because the contribution of polarization resistance is shifted by about 10% of the battery capacity. Figure 10 shows the decomposition of these parameters for the typical discharge curve. Now, we use these equations to build the single cell model in Simulink. The basic idea is using one input (i.e.,

current) to model the outputs (i.e., current, voltage and *SOC*). Figure 11 shows the detail of the constructed single cell model.

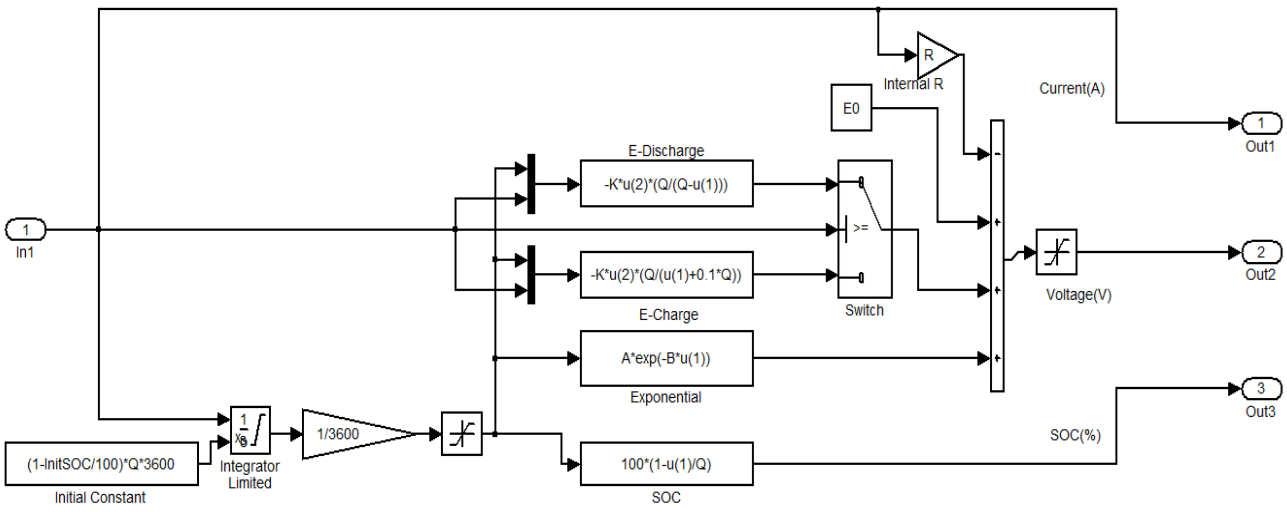

Figure 11 Single Cell Model

In this model, current just flows through the cell so the output current remains the same as the input. The voltage branch consists of four different modules corresponding to the four parts in the mathematical equations (3.1) and (3.2). In Figure 11, *R* represents the internal resistance and when multiplied by current this branch becomes one voltage component due to the internal resistance. E_0 is the base voltage of the cell. Discharging and charging are shown in two modules connected by a Switch Module. These two modules are expressed by the Function Module in Simulink.

Simulink is a data flow graphical programming language tool for modeling, simulating and analyzing multi-domain dynamic system (Simulink Manual). It offers tight integration with the rest of MATLAB environment and can either drive MATLAB or be scripted from it. The

advantage of Simulink is that it provides a graphical block diagramming tool which make the programming methods more clear to understand and design.

The last module in the voltage branch describes the exponential part. We use the Switch Module and the sign of the current value to control the current flow through the discharging or charging states. When the current in the branch is greater than or equal to zero, the switch will bridge to the discharging module. Otherwise, the switch will connect the charging module. Because the polarization resistance term in the equation contains two variables: current (I) and used capacity (D), we use Mux Modules to mix these two variables together as the input for the charge/discharge portion. The last branch of the single cell model is the *SOC* branch. We apply an Integrate Module to show the used capacity, $it = \int idt$, denoted by D, and then *SOC* can be represented by a percentage of the unused capacity over the total battery capacity.

Simulink has a very convenient function that can set variables' values when making the whole system a sub-system, see Figure 12. The Li-ion Cell sub-system in Figure 12 is actually the single cell model we just showed in Figure 11. In this "upper" system, we can easily define and change the parameters in the sub-system by right clicking on the Li-ion Cell system and choosing "Add Mask".

At the left-hand side of Figure 12, we set several different input modules (Constant Module with a positive value, Constant Module with negative value, Pulse Generator, and Uniform Random Number Module) to represent the power supply and working load modes in the charging and discharging states. At the right-hand side, we connect the three outputs to a scope to show the

profile of each variable so we can learn clearly the responses of these variables when the input mode is changed.

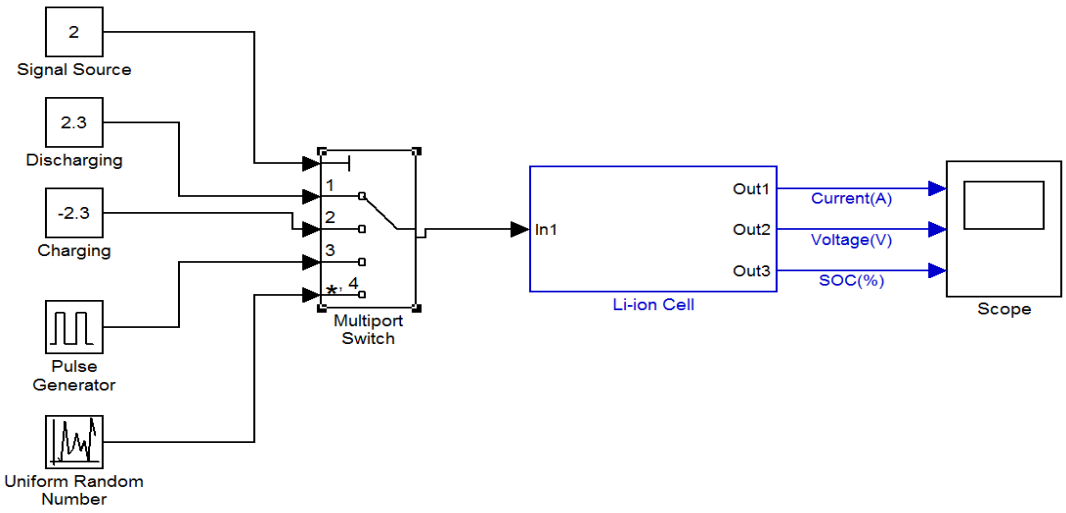

Figure 12 Main System of Single Cell Model

3.3 Dynamics Modeling of Battery Package System

Series and parallel connections are two most basic layouts in the packed battery. The welding process is used to physically connect two and more cells together. Welding points are introduced into the pack during the welding process. In this section, we will discuss these two basic connection layouts in details, build a model for each of them, and then expand the single-cell model to a more complex mixed connection layout involving both series and parallel connection elements for a multi-cell battery pack.

3.3.1 Serial Connection

A Simulink model is used to present the basic series connection layout in Figure 13. The model contains two single Li-ion cells connected in series. The inputs for these two cells are identical because the current (out1) does not change, and the outputs are similar to the single cell model except we added an additional output that represents the battery's capacity (*Q*). This *Q* can help us control the input in the *SOC* Collector module. In the series connection model, we use a Summation Module to show the voltage output(out2), because the voltage value in series connection should be doubled compared with a single cell. The *SOC* section is different from the single cell, the first two inputs are the cells' *SOCs* and the other two are the cells' capacities (*Qs*). The *SOC* can be represented by the cell's current capacity divided by the cell's total capacity.

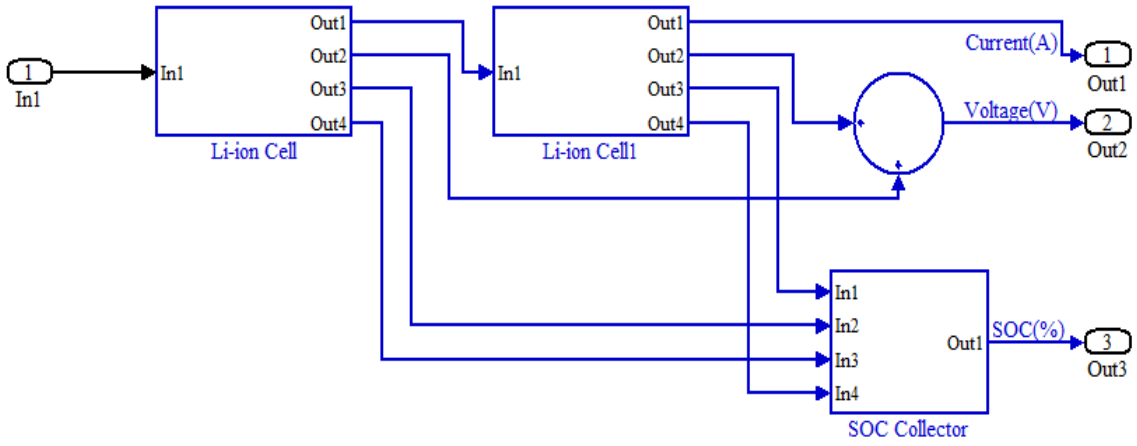

Figure 13 Series Connection Model of a Two-Cell Pack

Figure 14 is an illustration of the *SOC* Collector Module. In1 and In2 in Figure 14 represent cell 1's and cell 2's *SOCs* (%), respectively, while In3 and In4 represent cell 1's and cell 2's capacities (*Qs*) respectively. The equation applied in the Function Module is the representation of:

$$\begin{cases} SOC_1 = \dfrac{Q_1 - D_1}{Q_1} \\ SOC_2 = \dfrac{Q_2 - D_2}{Q_2} \end{cases} \tag{3.3}$$

where D_1 and D_2 indicate the used battery capacities of cells 1 and 2, respectively.

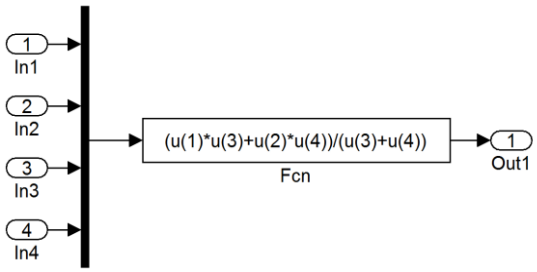

Figure 14 *SOC* Collector Model

3.3.2 Parallel Connection

Unlike the series connection model, the parallel connection needs to keep voltage the same while current changing with the increased or decreased number of cells in the pack. For illustration purposes, a three-cell parallel pack model is shown in Figure 15. All of the modules used in the parallel connection model have been introduced in the previous section except for the connection layout. Here the parallel connection aims to get the desired enlarged current value. To describe the current increasing, we set the input current as three times larger than the single cell, then we use three Function Models to evenly separate the current into each battery cell and at the end of the current branch, we set a Summation Module to implement the current increasing. For the voltage branch, three Function Modules are used to decrease the voltage in each cell. Let the voltage be equal to 1/n of the single cell's voltage, where n is the number of the cells in the pack,

and the resulting sum of these voltages is equal to single cell voltage so the parallel connection property can be obtained. The *SOC* Collector is similar but with two more inputs which represent the third cell's *SOC* and capacity *Q*.

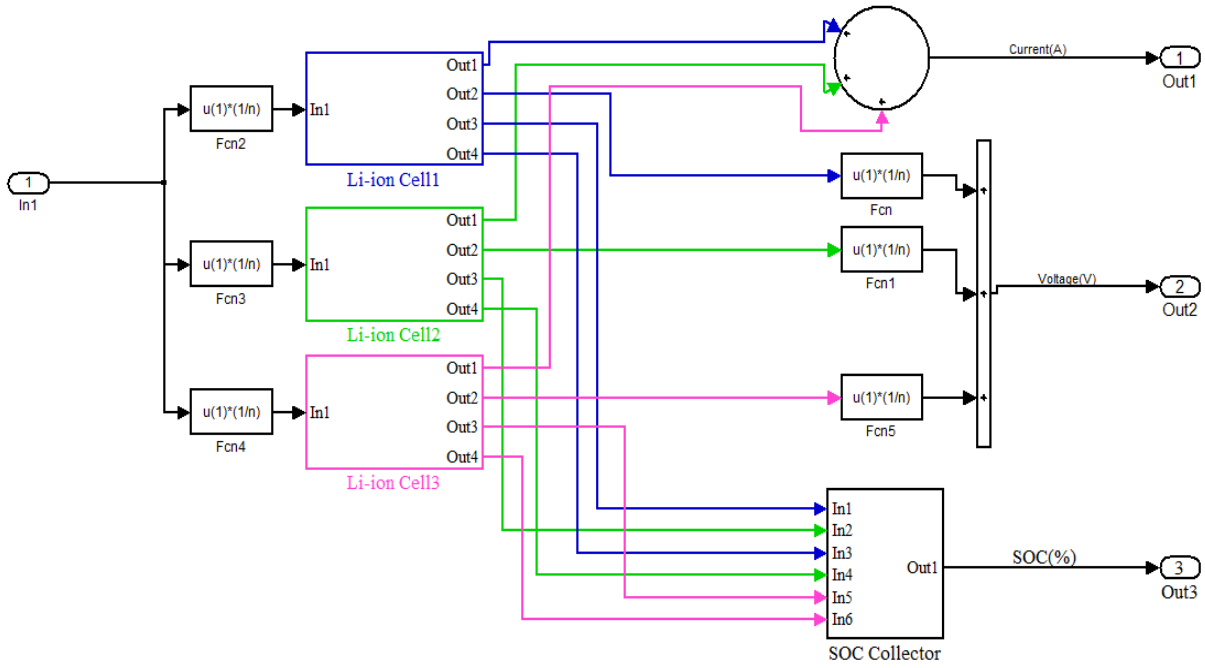

Figure 15 Parallel Connection Model of a Three-Cell Pack

3.3.3 Welding Point

The welding process is used to connect multiple cells together. There are several welding techniques adopted in the battery industry such as laser, ultra-sonic, nano-bond, and capacitive discharge. Although the welding techniques are becoming more and more mature, the welding points are still a main cause for the variability of performance of the packed battery. Different welding conditions (techniques, equipment, etc.) may result in different internal resistance. Therefore, a flexible welding point model is useful in battery pack modeling.

In this study, we introduce a welding point model into the Li-ion pack model by using Function Module as shown in Figure 16. We simply model the imperfect welding point using a deterministic value. However, of course it can be modeled with more complex space or time variations.

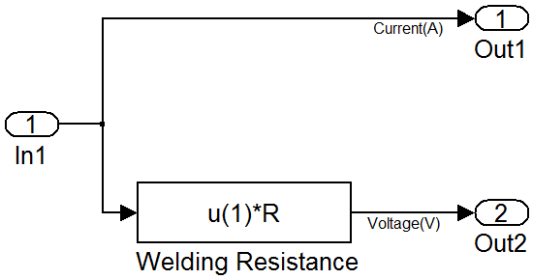

Figure 16 Welding Point Model

The series and parallel models are slightly modified to make the calculation of the *SOC* easier. Figures 17 and 18 show the serial and parallel connection models with welding points. These models are based on their mathematical relationships, not on their physical connections.

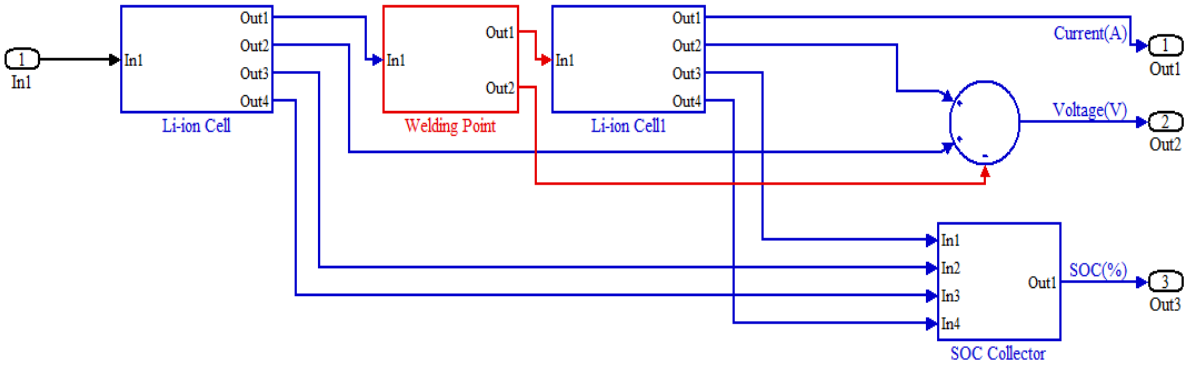

Figure 17 Series Connection Model with Welding Point

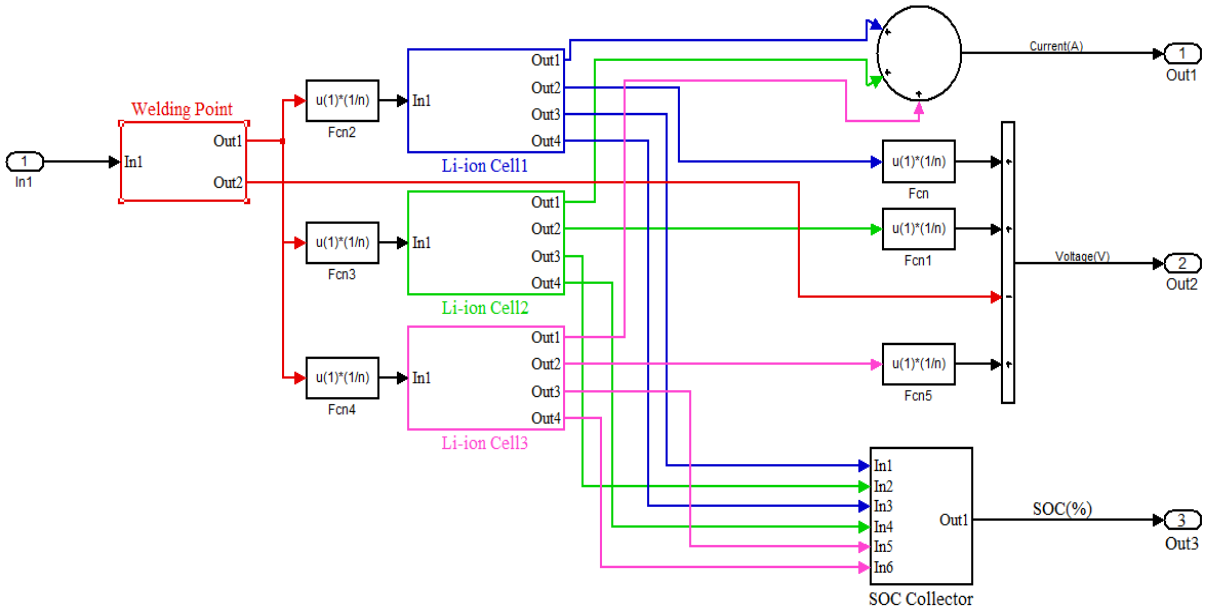

Figure 18 Parallel Connection Model with Welding Points

There is one welding point in the two-cell series model. Note that the welding points will cause a slight drop of the terminal voltage. We subtract this part from the total battery voltage by adding a minus sign into the Summation Module. For the parallel model, there are four welding points among the three cells and for the sake of convenience, we combine all of them into one module so that we can control the resistance value by double clicking the welding point module and changing the parameter in the interface showing up.

3.3.4 Multi-Cell Package Model

Now with the series and parallel connection models being ready, we can extend the models to create a multi-cell pack system. For example, for a nine-cell battery pack, the layout of this pack is three cells connected in parallel to form a unit and three such units connected in series to form the pack. There are fourteen welding points in this pack. The parallel connections are to help

increase the current in the whole system to reach the desired value, and the series connections are to help increase the voltage to reach the desired value.

3.4 Simulation-Based Model Validation

In this section, we illustrate how to determine the model parameters and provide the battery dynamic performance profile with different loads. The battery pack model will be validated.

3.4.1 Parameter Determination

In the cell charging/discharging dynamics equations (3.1) and (3.2), the current I, internal resistance R, battery capacity Q, and used capacity D are generally given by the manufacturers or can be easily calculated. However, the remaining four parameters E_0, a, b, and k should be determined mathematically. One of the important features of the mathematical model introduced in Section 3.2 is the simplicity of the parameter determination. Recall the typical discharging/charging curve in Figure 9. We can simply grab three points (as shown in Figure 19) on that curve to determine these parameters. Note that these three points are obtained in steady load condition (Tremblay, O and Dessaint, L. A 2009). The curves are generally available as the form of a data sheet provided by cell manufacturers.

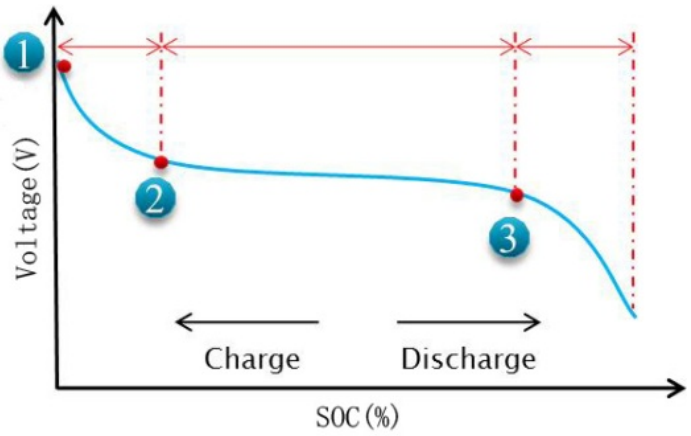

Figure 19 Model Parameters Determination Curve

According to Tremblay (Tremblay, O and Dessaint, L. A 2009), at point 1, it represents the cell state when it is fully charged so that the used battery capacity D_1 is zero. $\frac{Q}{Q-D}$ is the *SOC* (%) and at this point its value is one. The current is zero. According to equation (3.1), we have

$$V = E_0 + a \tag{3.4}$$

At point 2, the normal discharging begins just after the exponential part ends, which means the battery begins working normally. Now the voltage is

$$V = E_0 + a \cdot e^{-b \cdot D2} - I \cdot R - I \cdot k \frac{Q}{Q - D_2} \tag{3.5}$$

where D_2 is the used capacity at point 2, and I and R are the battery current and resistance, respectively. According to Tremblay (Tremblay, O and Dessaint, L. A 2009), b has an approximate relationship with used capacity as showing in equation (3.6):

$$b \approx 3 / D_2 \tag{3.6}$$

At point 3, the normal discharging almost ends, which means the battery has almost completely lost its charge. We obtain another equation

$$V = E_0 + a \cdot e^{-b \cdot D3} - I \cdot R - I \cdot k \frac{Q}{Q - D_3} \tag{3.7}$$

where D_3 is the used capacity at point 3.

Using the equations (3.4) to (3.7), we can get all the model parameters. In general, the more precise the points extracted from the curve are, the more accurate the obtained parameters are. The parameters for a common Li-ion battery with 3.3V rated voltage and 2.3Ah rated capacities are shown in Table 1.

Table 1 Battery Parameters

Parameters	Value
E_0 (V)	3.374
R(Ω)	0.014
a(V)	0.26422
b(Ah)$^{-1}$	26.5487
k(Ω or V/Ah)	0.0076

3.4.2 Validation of Li-ion Battery Pack Model

With the parameters we acquired in the last section, we can now validate the model numerically. We use the parameter-setting panel to set up the model parameter in Simulink. The resistance of

the welding point is assumed to be 0.014Ω. In reality, the welding resistances may differ from each other due to different welding techniques, operators, or machines. The comparisons of single, series, parallel cells' results are shown in Figure 20. Note the blue solid line in Figure 20 is the profile of the single cell model in Section 3.2, the red dashed line is the profile of series connection of two Li-ion cells in Section 3.3.1, and the green dot-dashed line is the profile of parallel connection of three Li-ion cells in Section 3.3.2. All battery models are undergone a 2.3A discharging current. Because the single cell has 2.3Ah rated capacity, the discharging will last for approximately one hour. We can see that the series connection model has the same current with the single cell model so that their discharging time is same. However, the voltage of the series connection is twice as large as the single cell's. There are three cells in the model of parallel connection, thus the discharging time is three times of which in the single cell model while the voltage of the two models keep the same. As a result, we can keep adding cells into the parallel system until we get the desired current value and then serially connect all these parallel systems together to obtain the voltage that can service the EV load.

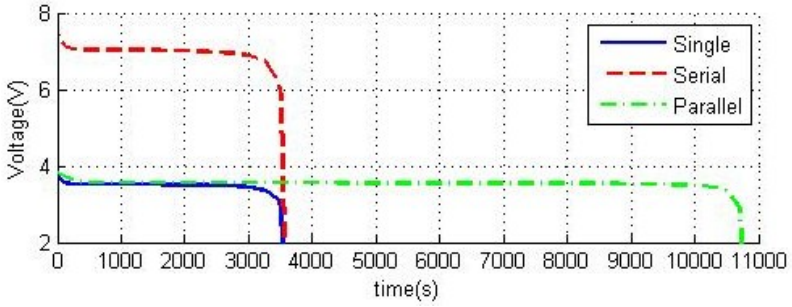

Figure 20 Comparisons of Li-ion Models

Now we consider the system with welding points. As mentioned in Section 3.3.3, welding points are an inevitable component in a battery pack. Although each of them may be very small, from the whole system's perspective, the resistance of welding points cannot be ignored due to the

influence they have on the system performance. Usually in an EV propulsion system, there are hundreds of cells in the battery pack, if every pair of cells needs one welding point for a series connection and two for a parallel connection, the number of welding points in the entire system becomes very large. Figures 21, 22 and 23 show the nine-cell simulation comparisons with and without welding points in different loading modes.

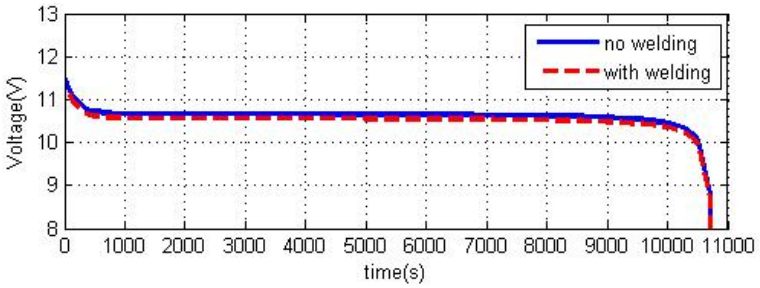

Figure 21 Discharging Curves of the Nine-Cell Pack with and without Welding Points (Constant Current)

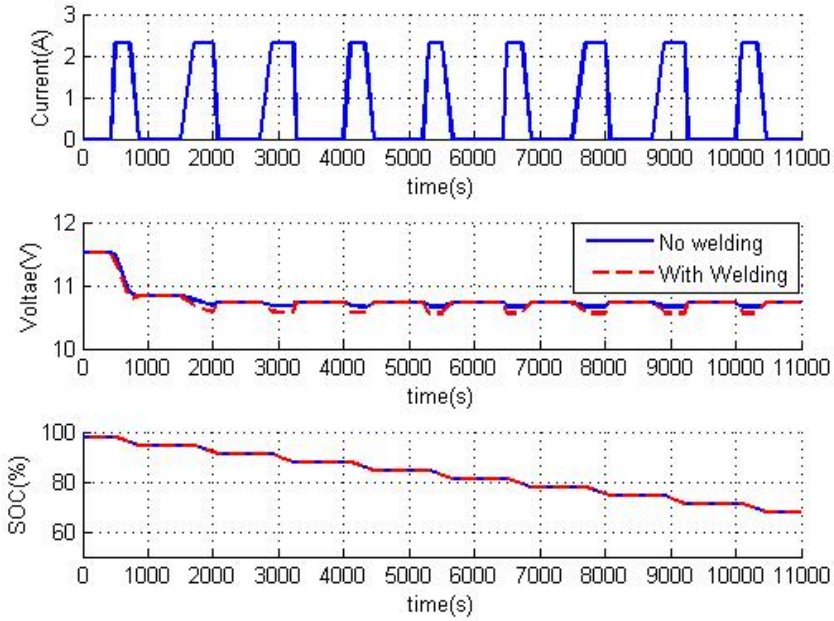

Figure 22 Discharging Curves of the Nine-Cell Pack with and without Welding Points (Pulse Generator Current)

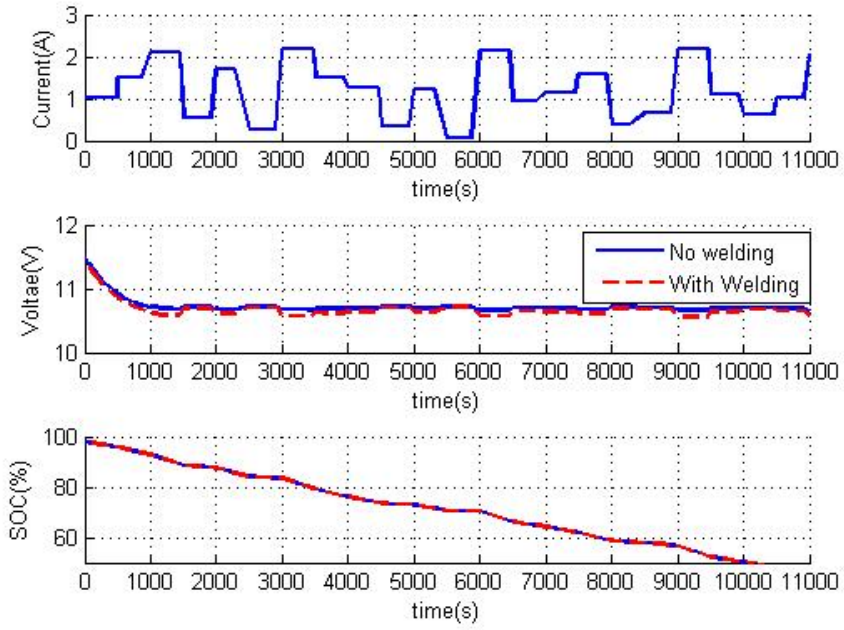

Figure 23 Discharging Curves of the Nine-Cell Pack with and without Welding Points (Uniform Random Generator Current)

These battery dynamic simulation profiles demonstrate the influence of the welding points on the performance of multi-cell battery system. As we can see from Figure 21, the voltage is generally lower for the system with welding points than the system without welding points. The same phenomenon displayed in Figures 22 and 23. Note that in our model, we assume the working environment such as temperature is in the ideal condition and kept the same for all the systems, so the models only describe the connection relationships but not include the supplemental components (e.g. cooling system, monitoring unit).

3.5 Conclusions

This chapter establishes a set of enhanced models that can represent the multi-cell battery dynamic behavior considering the influence of manufacturing processes. The Simulation models can generally reflect the real-time battery condition with different working loads. Three typical models including single Li-ion cell, series connection of two Li-ion cells and parallel connection of three Li-ion cells are provided. Finally, the multi-cell Li-ion battery pack model can be presented. In the case of a nine-cell battery pack, the welding points' influence on the entire battery system by comparing dynamic performances of the models with and without welding points after applying different loading modes is studied and the established models are validated.

4. BATTERY PACKAGE SYSTEM LAYOUT OPTIMIZATION

4.1 Introduction

Besides the pack-level working dynamics and performance evaluation for the BPS, the cost of the BPS is also a critical issue that may influence the further development of EV technology. In this chapter, we focus on an optimal layout design model for the BPS in terms of cost effectiveness based on a novel multi-capacity BPS structure that is composed of several independent parallel sub-systems which can be connected or disconnected based on different driving modes (load demand). We will first introduce our idea of the multi-capacity BPS briefly.

After that, the mathematical model for optimal layout design considering the proposed multi-capacity BPS will be established. The solution technique will be given and a numerical case study will be conducted to illustrate the effectiveness of the proposed methodology.

4.2 Multiple Capacity BPS

As is known to all, the vehicles may work under different driving modes, for example, when it is running on high-way, it requires more energy output than it is running in urban area. However, the capacity of the current vehicle BPS is constant depending on its largest demand, which means part of capacity is wasted when the BPS does not work under the full load. In this chapter, we define three different driving modes based on different frequencies, i.e., high, intermediate, and low. Without losing generality, we assume the energy demand for each driving mode is reverse to the frequency sequence, i.e., the most frequent driving mode with the lowest energy demand, etc. Also assume the BPS is able to determine which sub-systems to be activated or deactivated based on the sampled data that describe the driving modes. Figure 24 illustrates an example of multi-capacity BPS.

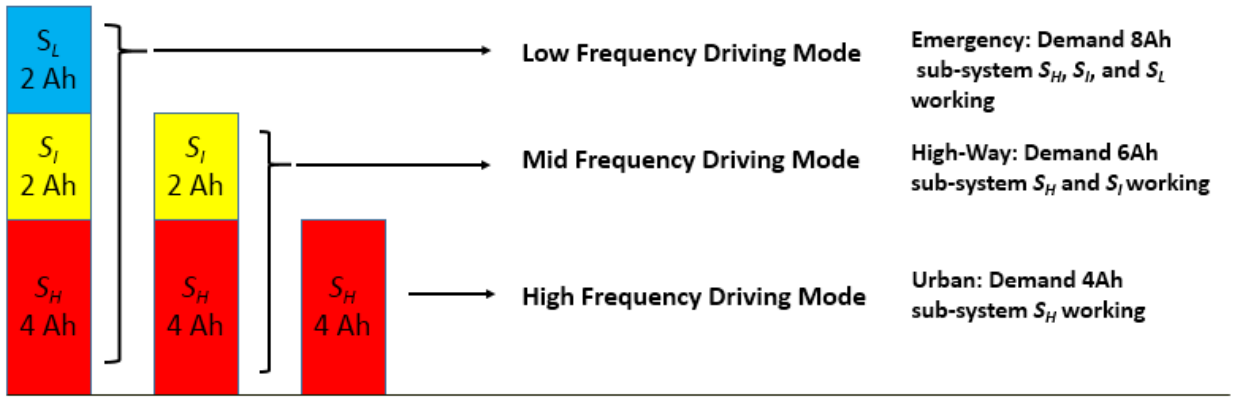

Figure 24 An Example of Multi-Capacity BPS Based on Three Driving Modes

In Figure 24, the BPS consists of three sub-systems, denoted by S_H, S_I, and S_L with different capacities and designed working frequencies. It can be seen that we may activate sub-system S_H to power the EV when driving in urban area with low energy demand; 2) we need activate the sub-system S_I along with sub-system S_H to obtain a higher energy output when driving on the high-way with higher energy demand; and 3) we have to activate sub-system S_L along with sub-system S_H and S_I to obtain enough energy output to meet the highest demand.

Intuitively, the type of battery cell used for the sub-system with high usage frequency prefers a larger lifecycle since it is expected to be charged and discharged more frequently. It means a higher first time purchase cost, however, the replacement cost during the lifetime of the vehicle may be reduced due to the extended lifetime. In contrast, the lower lifecycle configuration may lead to a lower first time purchase cost but a higher replacement cost during the lifetime of the vehicle. It incurs the tradeoff between the initial cost and the replacement cost. In this chapter, a mathematical model that describes the overall cost of the BPS during the lifetime of the vehicle will be established. The optimal layout design is identified by minimizing the overall cost under

the constraint that the probability of the BPS satisfies the demand is not lower than a predetermined value.

4.3 Methodology

4.3.1 Assumptions

1. The type of battery cells in same sub-system is identical.
2. Each sub-system of the BPS can be charged or discharged separately.
3. Each sub-system of the BPS can be replaced separately

4.3.2 Notations

i: index of sub-systems in the battery package, $i=H,I,L$

j: index of the type of cell

DR_H: driving mode with the highest frequency

DR_I: driving mode with the intermediate frequency

DR_L: driving mode with the lowest frequency

S_H : sub-system that need be activated to satisfy the most frequent driving mode DR_H

S_I : sub-system that need be activated along with S_H to satisfy the intermediate frequent driving mode DR_I

S_L : sub-system that need be activated along with S_H and S_I to satisfy the least frequent driving mode DR_L

PR_H: probability that under the driving mode DR_H

PR_I: probability that under the driving mode DR_I

PR_L: probability that under the driving mode DR_L

F_H: cumulative probability that S_H will be used, $F_H = PR_H + PR_I + PR_L = 1$

F_I: cumulative probability that S_I will be used, $F_I = PR_I + PR_L$

F_L: cumulative probability that S_L will be used, $F_L = PR_L$

D_{HF}: cumulative energy demand (Ah) by the most frequent driving mode DR_H

D_{IF}: cumulative energy demand (Ah) by the intermediate frequent driving mode DR_I

D_{LF}: cumulative energy demand (Ah) by the least frequent driving mode DR_L (Assume $D_{HF} \le D_{IF} \le D_{LF}$)

D_L: incremental demand (Ah) when driving mode shifted from DR_I to DR_L, $D_L = D_{LF} - D_{IF}$

D_I: incremental demand (Ah) when driving mode shifted from DR_H to DR_I, $D_I = D_{IF} - D_{HF}$

D_H: incremental demand (Ah) for driving mode DR_H, $D_H = D_{HF}$

G_{Hj}: expected output capacity of sub-system S_H that consists of type *j* cells

G_{Ij}: expected output capacity of sub-system S_I that consists of type *j* cells

G_{Lj}: expected output capacity of sub-system S_L that consists of type *j* cells

M: average driving miles per year

LC_{ij}: lifecycle of the sub-system *i* consisting of type *j* cells

U_H: average miles of driving per each charging-discharging cycle for sub-system S_H

U_I: average miles of driving per each charging-discharging cycle for sub-system S_I

$$U_I = U_H \cdot \frac{F_H}{F_I} \tag{4.1}$$

U_L : average miles of driving per each charging-discharging cycle for sub-system S_L

$$U_L = U_H \cdot \frac{F_H}{F_L} \tag{4.2}$$

Y: expected lifetime of the vehicle

CY_{ij} : expected lifetime (in years) of the sub-system i consisting of type j cells

CN_{ij} : expected change time for the sub-system i consisting of type j cells during the vehicle lifetime Y

g_{ij} : capacity of type j cell in sub-system i

r_{ij} : reliability of type j cell in sub-system i

c_{ij} : cost of type j cell in sub-system i

x_{ij} : number of type j cells used in sub-system i

β_y : nominal interest rate per year compounded monthly

γ_y : effective rate per year

$\gamma_{CY_{ij}}$: effective rate for the period with the duration CY_{ij} years

4.3.3 Problem Formulation

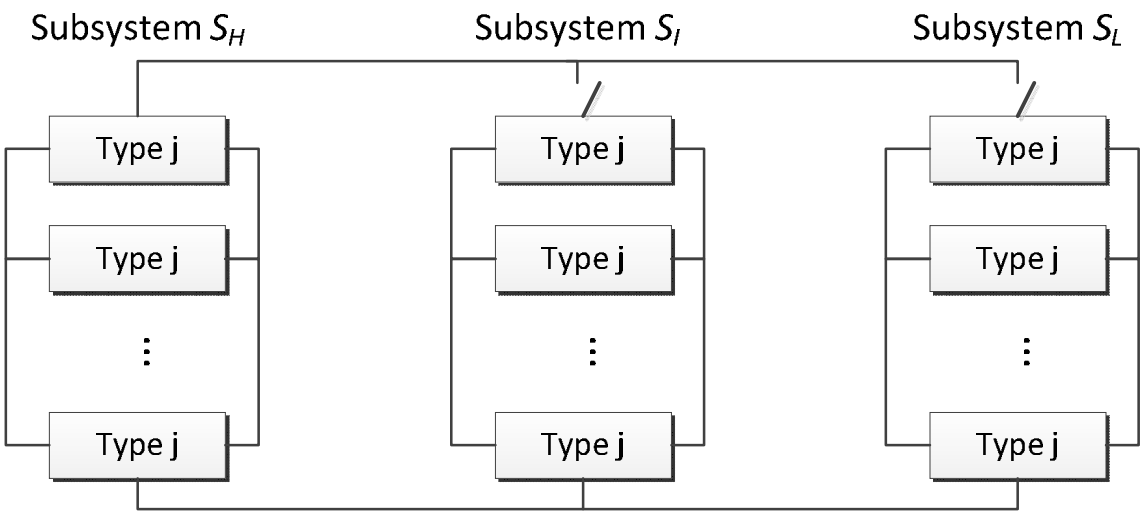

Figure 25 Layout of Multi-Capacity BPS with Three Sub-Systems

Figure 25 shows the structure of the multi-capacity BPS proposed in Section 4.2. The BPS consists of three sub-systems in parallel. Within each sub-system *i*, same type *j* battery cells with equivalent functionality are connected in parallel. The cost for sub-system *i* consisting of type *j* cells can be described by (4.3).

$$C_{ij} = \sum_{j} x_{ij} \cdot c_{ij} \tag{4.3}$$

where the subscript *j* of C_{ij} is determined by the subscript of the non-zero variable x_{ij}.

The expected lifetime CY_{ij} (in years) of the sub-system *i* consisting of type *j* cells can be described by (4.4).

$$CY_{ij} = \frac{LC_{ij} \cdot U_i}{M \cdot F_i} \tag{4.4}$$

The expected replacement time for the sub-system *i* consisting of type *j* cells during the vehicle lifetime Y CN_{ij} can be described by (4.5).

$$CN_{ij} = \frac{Y}{CY_{ij}} = \frac{Y \cdot M \cdot F_i}{LC_{ij} \cdot U_i} \tag{4.5}$$

The estimated salvage value for the sub-system *i* consisting of type *j* cells at the end of the life of the vehicle R_{ij} can be described by (4.6).

$$R_{ij} = \frac{[\lceil CN_{ij} \rceil \cdot CY_{ij} - Y]}{CY_{ij}} \cdot C_{ij} \tag{4.6}$$

Let β_y be the nominal interest rate per year compounded monthly. The effective rate per year γ_y can be described by (4.7).

$$\gamma_y = [1 + (\frac{\beta_y}{12})]^{12} - 1 \tag{4.7}$$

Let $\gamma_{CY_{ij}}$ be the effective rate for the period with the duration CY_{ij}, which can be described by (4.8).

$$\gamma_{CY_{ij}} = [1 + (\frac{\beta_y}{12})]^{12 \cdot CY_{ij}} - 1 \tag{4.8}$$

The present value of the expected cost for sub-system *i* consisting of type *j* cells can be described by (4.9).

$$TC_{ij} = \sum_{k=0}^{\lfloor CN_{ij} \rfloor} \frac{C_{ij}}{(1+\gamma_{CY_{ij}})^k} - \frac{R_{ij}}{(1+\gamma_y)^Y} \tag{4.9}$$

The objective function can be described by (4.10).

$$\min_{x_{ij}} TC = \min_{x_{ij}} \sum_i \sum_j TC_{ij} \tag{4.10}$$

Several constraints are described as follows:

1) Let P_S be the probability that the BPS satisfies the demand. It need be larger than a threshold value P_0, which can be described by (4.11).

$$P_S = \prod_i P_i(G_{ij} \geq D_i) \geq P_0 \tag{4.11}$$

where

$$P_i(G_{ij} \geq D_i) = \begin{cases} 1-(1-r_{ij})^{x_{ij}} & \text{if } D_i \leq g_{ij}, \\ 1-b(x_{ij},1,r_{ij}) & \text{if } g_{ij} < D_i \leq 2g_{ij}, \\ \ldots & \ldots \\ 1-b(x_{ij},k-1,r_{ij}) & \text{if } (k\text{-}1)g_{ij} < D_i \leq kg_{ij}, \\ \ldots & \ldots \\ r_{ij}^{xij} & \text{if } (x_{ij}\text{-}1)g_{ij} < D_i \leq x_{ij}g_{ij}, \\ 0 & \text{otherwise.} \end{cases} \tag{4.12}$$

2) The constraint of the minimum cell number in each sub-system can be described by (4.13).

$$x_{ij} \geq D_i / g_{ij} \tag{4.13}$$

3) Homogenous constraint can be described by (4.14).

$$x_{ij}x_{ip} = 0, \forall i \text{ and } j \neq p, x_{ij} \in Z^+ \tag{4.14}$$

4) For different sub-systems, due to the different charging-discharging frequency, the cell selection need consider the different criteria of the number of lifecycles. It can be described by (4.15).

$$LC_{ij} \geq LC_{i0} \tag{4.15}$$

where LC_{i0} is the threshold value of the life cycles for sub-system *i*.

4.3.4 Solution Technique: Brute-Force Search Optimization

Brute-Force Search (BFS) will be used to solve the optimization model proposed in Section 4.3.3. BFS is a very famous and general problem-solving method for optimization. BFS consists of systematically enumerating all possible candidate solutions for the problem and checking whether each solution satisfies the problem statement and constraints. While BFS algorithm is simple to implement and can always find a solution if there is one existing, but the cost is the candidate solutions can increase proportionally. In reality, the problems tend to grow very quickly as the size of the problem increase, this will lead to the search time for the optimal solution incredible enlarged. Therefore, BFS is typically used when the problem size is limited and small, or when there are problem-specific heuristics that can be used to reduce the set of candidate solutions to a manageable size. BFS also can be used when the simplicity of implementation is more important than search speed.

To conduct a BFS, there are four steps need be processed, namely: Initialization, Iteration, Validation and Output. For example, if the problem we are dealing with can be defined as *S*, then following procedures can be used to conduct BFS:

1) Initialize (*S*): generate a first candidate solution for problem *S*.
2) Iteration (*S*, *i*): generate the next candidate solution for problem *S* and compare with the current solution *i*, replace *i* if the new solution is better the current one.
3) Validation (*S*, *i*): check whether the solution is feasible or not for problem *S*.
4) Output (*S*, *i*): use the feasible solution *i* as the appropriate solution of problem *S*.

4.4 Case Study

4.4.1 Problem Description

In order to validate the algorithms introduced in Section 4.3, a numerical case study focusing on a multi-capacity BPS with three sub-systems is conducted. The layout of the BPS is shown in Figure 25.

The parameters of different types of cells available for the BPS are shown in Table 2. The cost, cell capacity, reliability, and life cycle times are illustrated. The parameters for different driving modes are illustrated in Table 3. Other key parameters are shown in Table 4.

Table 2 Li-ion Battery Cells Specifications

Sub-system	*Minimum Life Cycles (LC_{i0})*	*Cell Type*	*Capacity (g_{ij})*	*Reliability (r_{ij})*	*Life Cycle (LC_{ij})*	*Cost (c_{ij})*
S_H	580	1	1420	0.97	620	1.19
		2	1270	0.964	600	1.02
		3	1200	0.960	590	0.99
		4	1000	0.95	580	0.936
S_I	400	5	830	0.927	450	0.835
		6	810	0.914	430	0.813
		7	780	0.96	400	0.783
S_L	300	8	400	0.949	320	0.42
		9	350	0.959	300	0.49

Table 3 Parameters for Different Driving Modes

Driving Mode	*Incremental Demand (D_i)*	*Cumulative Demand (D_{iF})*	*Probability of Usage (PR_i)*	*Cumulative Probability of Usage (F_i)*
DR_H	4 Ah	4 Ah	40%	100%
DR_I	2 Ah	6 Ah	35%	60%
DR_L	2 Ah	8 Ah	25%	25%

Table 4 Other Key Parameters

Parameters	*Values*
β	1%
M	10000 miles
U_H	80 miles
Y	10 years

4.4.2 Results and Discussions

Following the technique in Section 4.3.4, the optimal results based on different values of P_0 are obtained as shown in Table 5. The solution is composed of six numbers. The first, third, and fifth number represent the type of cell used for sub-system S_H, S_I, and S_L, respectively. The second, fourth, and sixth number represent the respective number of cells used in corresponding sub-systems.

Table 5 Optimal BPS Layout with Different P_0 values

Best Solutions	P_0	*Cost*	P_S
[1,3;3,2;4,3]	0.900	13.4876	0.9297
[1,3;4,3;4,3]	0.950	14.4870	0.9829
[1,3;4,3;3,3]	0.985	14.5228	0.9873
[1,3;3,3;3,3]	0.990	14.6538	0.9917
[1,3;4,4;8,5]	0.995	15.6889	0.9957

Table 6 Comparison of the Cost of the Optimal Layout between the Multi-Type Cell and Single Type Cell Configuration with P_0=0.985

Solution (X)	*Cost*		
	Multi-Type	Single-Type	Cost Improvement (%)
[2,3,4,3,3,3]	14.5228	-	-
[1,3;1,3;1,3]	-	15.2795	4.95
[2,4;2,4;2,4]	-	18.0269	19.4
[3,4;3,4;3,4]	-	17.7838	18.3
[4,4;4,4;4,4]	-	17.0941	15.0
[5,5;5,5;5,5]	-	24.3332	40.3
[6,5;6,5;6,5]	-	28.1722	48.4
[7,6;7,6;7,6]	-	30.6807	52.7
[8,10;8,10;8,10]	-	34.0560	57.4
[9,12;9,12;9,12]	-	50.7931	71.4

Table 6 illustrates the comparison of the cost between the layout designed by the proposed method in this chapter, i.e., the criteria of the lifecycle of cells for different sub-systems are different, and the layout where same type cells are used for the whole BPS under the constraint

that the probability that the BPS satisfies the demand cannot be lower than 0.985. It can be seen the proposed methodology outperforms the traditional same type configuration.

4.5 Conclusions

In this chapter, we propose a multi-capacity BPS system that can adjust the output energy based on different driving modes. Based on this idea, a cost-effective BPS layout design model is introduced considering different cell types used for different sub-systems of the BPS. The results of the numerical case study illustrates the cost reduction can be achieved by the proposed method compared to traditional method that the whole BPS consists of the cells with the same type.

5. CONCLUSIONS AND FUTURE WORK

In this thesis, a simulation model to investigate the dynamics behavior and evaluate the working performance of BPS is established. Typical profiles of battery discharge/charge and State of Charge for different connections with different manufacturing processes can be obtained by the proposed model. A nine multi-cell BPS system is used to show the validation of the simulation model.

After that, an optimal layout design model which aims to identifying the best layout with the minimized overall cost considering the novel idea of multi-capacity BPS is introduced. Separate sub-systems that can be separately charged/discharged and replaced/maintained are proposed. Different cell types are considered for different sub-systems of the BPS. The results of the numerical case study show that the total cost can be effectively reduced compared with traditional layout design idea that the whole BPS consists of the cells with the same type.

For the future work, we first plan to apply the developed models for the applications of the system with real size of cells. More complex solution algorithm with acceptable computational cost will be tried. We also plan to integrate real driving condition and driver's profile (Wu, C. and Wan, J. 2012) and conduct real experiments to further validate the effectiveness of the established models.

REFERENCE

1. Aifantis, K. E., Hackney, S. A., Dempsey, J. P., 2007, "Design Criteria for Nanostructured Li-ion Batteries", Journal of Power Sources, Vol. 165, pp. 874-879.

2. Agarwal, M. and Gupta, R., 2007, "Homogeneous Redundancy Optimization in Multi-State Series-Parallel Systems: A Heuristic Approach", IIE Transaction, Vol. 39, pp. 277-289.

3. Bradley, T. H. and Frank, A. A., 2009, "Design, Demonstration and Sustainability Impact Assessments for Plug-in Hybrid Electric Vehicles", Renewable & Sustainable Energy Reviews, Vol. 13, pp. 115-128.

4. Chen, M. and Rincon-Mora, G., 2006, "Accurate Electrical Battery Model Capable of Predicting, Runtime and I-V Performance", IEEE Transaction on Energy Contype, Vol. 21, pp. 504-511.

5. Chen, M. and Rincon-Mora, G., 2006, "Accurate, Compact and Power-Efficient Li-ion Battery Charger Circuit", IEEE Transaction on Circuits and Systems II-Express Briefs, Vol. 53, pp. 1180-1184.

6. Einhorn, M., Roessler, W. and Fleig, J., 2011, "Improved Performance of Serially Connected Li-ion Batteries with Active Cell Balancing in Electric Vehicles", IEEE Transactions on Vehicular Technology, Vol. 60, pp. 2448-2457.

7. Guerrero, C. P. A., Li, J, Biller, S. and Xiao, G., 2010, "Hybrid/Electric Vehicle Battery Manufacturing: The State-of-the-Art", IEEE Conference on Automation Science and Engineering, Toronto, Ontario, Canada.

8. Girishkumar, G., McCloskey, B., Luntz, A. C., 2010, "Lithium-Air Battery: Promise and Challenges", Journal of Physical Chemistry Letters, Vol. 1, pp. 2193-2203.

9. Jossen, A., 2006, "Fundamentals of Battery Dynamics" Journal of Power Sources, Vol. 154, pp. 530-538.

10. Johnson, B. A. and White, R. E., 1998, "Characterization of Commercially Available Lithium-ion Batteries", Journal of Power Sources, Vol. 70, pp.48-54.

11. Ju, F., Wang, J., Li, J., Biller, S. and Xiao, G., 2011, "Virtual Battery: A Simulation Framework for Batteries in Electric Vehicles", IEEE Conference on Automation Science and Engineering, Trieste, Italy.

12. Kaiser, R., 2007, "Optimized Battery-Management System to Improve Storage Lifetime in Renewable Energy Systems", Journal of Power Sources, Vol. 168, pp. 58-65.

13. Knauff, M. and McLaughlin, J., 2007, “Simulink Model of a Lithium-Ion Battery for the Hybrid Power System Test bed”, Proceedings of the ASNE Intelligent Ships Symposium, Philadelphia, PA, USA.

14. Karner, D. and Francfort, J., 2007, “Hybrid and Plug-in Hybrid Electric Vehicle Performance Testing by the US Department of Energy Advanced Vehicle Testing Activity”, Journal of Power Sources, Vol. 174, pp. 69-75.

15. Lisnianski, A., Levitin, G., Ben-Haim, H. and Elmakis, D., 1996, “Power System Structure Optimization Subject to Reliability Constraints”, Electric Power System Research, Vol. 39, pp.145-152.

16. Levitin, G., Lisnianski, A., Elmakis, D., 1997, “Structure Optimization of Power System with Different Redundant Elements”, Electric Power Systems Research, Vol. 43, pp. 19-27.

17. Lee, Y. S. and Cheng, M. W., 2005, “Intelligent Control Battery Equalization for Series Connected Lithium-ion Battery Strings”, IEEE Transactions on Industrial Electronics, Vol. 52, pp. 1297-1307.

18. Martínez-Rosas, E., Vasquez-Medrano, R. and Flores-Tlacuahuac, A., 2011,“Modeling and Simulation of Lithium-ion Batteries”, Computers and Chemical Engineering, Vol. 35, pp. 1937-1948.

19. Miller, G., Studyvin, W., and Shimp, P., 2006, "Cell Equalization of Lithium Ion Cells," Power Systems Conference, New Orleans, LA, USA.

20. Manenti, A., Abba, A., Merati, A., Savaresi, S. M. and Geraci, A., 2011, “A New BMS Architecture Based on Cell Redundancy”, IEEE Transaction on Industrial Electronics, Vol. 58, pp. 4314-4322.

21. Plett, G., 2004, “High-Performance Battery-Pack Power Estimation Using A Dynamic Cell Model”, IEEE Transactions On Vehicular Technology, Vol. 53, pp. 1586-1593.

22. Shepherd, C. M., 1965,“Design of Primary and Secondary Cells, I: Effect of the Polarization and Resistance on Cell Characteristics”, Journal of the Electrochemical Society, pp.252-257.

23. Shepherd, C. M., 1965, “Design of Primary and Secondary Cells, II: An Equation Describing battery Discharge”, Journal of the Electrochemical Society, pp.657-664.

24. SAE Magazine, 2011, Chevrolet Volt Development Story.

25. Simulink Manual Book, 2011.

26. Tremblay, O. and Dessaint, L. A., 2009, “Experimental Validation of a Battery Dynamic Model for EV Applications”, World Electric Vehicle Journal, Vol.3.

27. Tremblay, O. and Dessaint, L. A., 2007,"A Generic Battery Modelfor the Dynamic Simulation of Hybrid Electric Vehicles", World Electric Journal, pp. 284-289.

28. Wu, C. and Wan, J., 2012, "Addressing Human Factorsin Electric Vehicle Design: Buildingan Integrated Computational Human-Electric Vehicle Framework", Journal of Power Sources, Vol. 214, pp. 319-329.

29. Wang, Y. and Li, L., 2012, "Heterogeneous Redundancy Allocation for Series-parallel Multi-States Systems Using Hybrid Particle Swarm Optimization and Local Search", IEEE Transaction on System, Man and Cybernetics-Part A: Systems and Humans. Vol. 42, pp.464-474.

30. Wikipedia contributors. 2013. "Battery History." Wikipedia, the Free Encyclopedia. Wikimedia Foundation, Inc.

VITA

NAME:	Chongye Wang
EUDCATION:	B.Eng., Industrial Design, Tianjin University of Commerce, Tianjin, P.R.China, 2010.
	M.S., Industrial Engineering, University of Illinois at Chicago, Chicago, Illinois, 2013.
EXPERIENCE:	Continuous Improvement Internship, Chiquita Brands Co., Ltd, Chicago, IL, USA, 2013.
	Assistant Engineer, Heuft Systems Technology (Germany) Co., Ltd, Shanghai, P.R. China, 2010.
	Auxiliary Designer as Internship, Maco Design (Shanghai) Co., Ltd, Shanghai, P.R China, 2010.
PROJECTS:	Hybrid Electric Vehicle Consumption Forecasting Using Time Series Analysis Based on CO2 Emission and Crude Oil Price in U.S.
	Gas Station Analysis Using Discrete Event Simulation.
PROFESSIONAL MEMBERSHIPS:	Student Member of Institute of Industrial Engineering. 2012 - 2013
PUBLICATIONS:	Chongye Wang, Yong Wang, Lin Li, Hua Shao, and Changxu Wu, 2013. Dynamic Modeling of Multi-Cell Lithium-ion battery Packs for Electric Vehicles Considering Effects of Manufacturing Processes, In Proceedings of 2013 ASME MSEC, Jun. 10-14, Madison, WI, USA.